



UNIVERSITY OF LEEDS

This is a repository copy of *Design, Fabrication and Characterization of Low Speed Open-jet Wind Tunnel*.

White Rose Research Online URL for this paper:
<http://eprints.whiterose.ac.uk/99364/>

Version: Accepted Version

Proceedings Paper:

Azzawi, IDJ, Mao, X and Jaworski, AJ (2016) Design, Fabrication and Characterization of Low Speed Open-jet Wind Tunnel. In: Ao, SI, Gelman, L, Hukins, DWL, Hunter, A and Korsunsky, AM, (eds.) Proceedings of World Congress on Engineering 2016. World Congress on Engineering 2016, 29 Jun - 01 Jul 2016, London, UK. Newswood Limited , pp. 883-888. ISBN 978-988-14048-0-0

This is an author produced version of a conference paper accepted for publication in the Proceedings of World Congress on Engineering 2016. Uploaded with permission from the publisher.

Reuse

Unless indicated otherwise, fulltext items are protected by copyright with all rights reserved. The copyright exception in section 29 of the Copyright, Designs and Patents Act 1988 allows the making of a single copy solely for the purpose of non-commercial research or private study within the limits of fair dealing. The publisher or other rights-holder may allow further reproduction and re-use of this version - refer to the White Rose Research Online record for this item. Where records identify the publisher as the copyright holder, users can verify any specific terms of use on the publisher's website.

Takedown

If you consider content in White Rose Research Online to be in breach of UK law, please notify us by emailing eprints@whiterose.ac.uk including the URL of the record and the reason for the withdrawal request.



eprints@whiterose.ac.uk
<https://eprints.whiterose.ac.uk/>

Design, Fabrication and Characterization of Low Speed Open-jet Wind Tunnel

Itimad D. J. AZZAWI, Xiaolan MAO and Artur J. JAWORSKI

Abstract— A new low-speed open-jet wind tunnel has been designed and constructed at the University of Leeds. A series of Computational Fluid Dynamics (CFD) and experimental evaluations were conducted to determine the flow quality and to verify the wind tunnel suitability for aerodynamic studies. Two sets of results are presented in the current paper. Initially, mean velocity and turbulent intensity measurements in an empty test section using a Pitot-static tube and hot wire anemometer (HWA) were introduced. These results show that flow quality was significantly affected by boundary layer controllers (honeycomb and mesh screens) in the settling chamber and wide angle diffuser. Investigations were also conducted to evaluate the effectiveness of using an array of synthetic jet actuators (SJAs) for flow control in a wake behind a convex "hump" model (section of circular cylinder). These additional tests were conducted to validate the suitability of the wind tunnel for aerodynamics research.

Index Terms—Open-jet wind tunnel design, CFD, SJA, and PSD.

I. INTRODUCTION

THE science of aerodynamics concentrates on studying the impact of airflow on solid objects. Wind tunnels designed to accommodate variety of models are essential part of aerodynamics research. The subjects of aerodynamic studies are effectively investigated through the use of wind tunnels, as wind tunnels are capable of simulating realistic airflow conditions through the test section. However, despite the applicability of wind tunnels, there are constraints in terms of their cost, size and limited understanding of their design [1]. The two major types of wind tunnel that generate airflow at specified speed are closed-circuit and open-circuit. In the case of the latter, the test section can be either enclosed by physical boundaries or open (so called "open-jet" wind tunnels).

There are several components in a typical wind tunnel; the contraction, test section and diffuser being the key parts. The contraction component significantly increases airflow velocity prior to entering the test section; wind tunnels generally should have contraction ratios of 6-9 [2].

Manuscript received March 6, 2016; revised April 16, 2016. Itimad DJ Azzawi is sponsored by Ministry of Higher Education & University of Diyala in Iraq (NO: 10-2374 HCED).

Itimad Azzawi is with the Faculty of Engineering, University of Leeds, Leeds LS2 9JT, UK; (e-mail: mmidja@leeds.ac.uk).

Xiaolan Mao is with the Faculty of Engineering, University of Leeds, Leeds LS2 9JT, UK; (e-mail: x.mao@leeds.ac.uk).

Artur J. Jaworski, the corresponding author, is with the Faculty of Engineering, University of Leeds, Leeds LS2 9JT, UK; (e-mail: a.j.jaworski@leeds.ac.uk).

The test section houses the test object during the study and typically, the test object dictates the size of the test section. Wide-angle diffusers in an open-jet wind tunnel are designed to slow airflow velocity. Due to the wide variety of tunnel designs and the lack of understanding of flow through wind tunnel constituents such as the wide angle diffuser, mesh screens and the blower itself, it is difficult to formulate prescriptive rules for wind tunnel design a priori.

II. OVERVIEW OF WIND TUNNEL DESIGNS

Over the last decade, CFD modelling has seen widespread growth in aerodynamics and wind engineering research [3, 4, and 5]. There is a tendency for computational models to run parallel with physics for the purposes of substantiating validated information. **Table I** outlines an overview of previous studies conducted using CFD to assess open-jet and closed wind tunnels.

Table I: Tabulated previous studies of subsonic wind tunnel facilities.

References	Location	Circuit type	Application	Speed (m/s)
[6]	Bangkok, Thailand	Open jet (Blower)	Fluid-dynamic research	30
[7]	Gorgia, Atlantic	Open jet (Blower)	Turbulent boundary layer studies	1.8 – 12.1
[8]	Stanford, California	Open jet (Blower)	Boundary-layer interaction	27
[9]	Stanford, California	Open jet (Blower)	Turbulent boundary layers studies.	7
[10]	University of Sheffield, UK	Closed	Fluid-dynamic research	10
University of Leeds	Leeds, (UK)	Open jet (Blower)	Fluid-dynamic research	3-23

This paper pertains to the development of an open-jet subsonic wind tunnel at the University of Leeds. Initially, the pressure losses were calculated for each component. Then all the losses were added up to determine the overall pressure loss of the entire circuit. This helps to determine the power needed for the wind tunnel operation. This calculation technique is compatible with both open and closed-circuit wind tunnels. Subsequently, Computational Fluid Dynamics (CFD) and experimental analysis were presented as a basis for comparison of the airflow properties through the wind tunnel test section. Finally, investigations were also conducted to evaluate the effectiveness of using an array of synthetic jet actuators (SJAs) in altering the velocity deficit in the wake flow behind a convex hump model. This wake area was represented in terms of fluctuating velocity (Urms)

and power spectral density (PSD) in the wake flow in both actuated and un-actuated convex hump flow field. These were additional experimental tests carried out to validate the suitability of the wind tunnel for further aerodynamic studies.

III. WIND TUNNEL CONFIGURATION

A Woodhook Ltd centrifugal fan (with backward-facing aerofoil-type blades) with a 5.5 kW and 1.5 HP electric motor was used to drive the open-jet wind tunnel. This fan can deliver a flow rate of up to 6.25 m³/s against static pressure of up to 650 Pa. The fan can be operated at several ranges of frequencies using a variable frequency inverter, from 5 Hz up to 50 Hz. This blower supplies air into a wide angle diffuser through rectangular to a square transition duct. The diffuser is simply designed of two parts connected in the middle through a bolted flange. The first diffuser part expands from 80×80 cm² to 110×110 cm² over a length of 50 cm, and an area ratio of 1.89. The second diffuser part expands from 110×110 cm² to 140×140 cm² over a length of 50 cm, giving a maximum angle of 33.4° and an area ratio of 1.61. Two screens with a porosity of 0.67 are placed in the middle between the two diffusers. A settling chamber is used to merge the airflow of two branches before it passes through the contraction segment of the wind tunnel. The honeycomb and screens are its two main constituents. The honeycomb with a thickness of 100 mm is placed at the inlet of the settling chamber. Sufficient space must exist between the screens to allow the flow pressure to restore itself from the perturbation caused by the movement of the flow through one screen to the following one. The ideal spacing is considered to be 0.2 of its width [1]. Therefore, a settling chamber with a 500 mm width needs about 100 mm spacing between each screen (three in total). This should also be the dimension of the space between the last screen and the contraction. The merged flow passes through the contraction section. The contraction has a square cross section of 140×140 cm² at an inlet, 50×50 cm² at the exit, and a contraction ratio (CR) of 7.8:1 that is in agreement with the recommended contraction ratio (6:9) [12, 13]; over a length (L) of 140 cm. The final construction of the wind tunnel is shown in **Fig.1**.



Fig. 1: The constructed open-jet wind tunnel

IV. NUMERICAL METHODOLOGY AND GOVERNING EQUATIONS

The numerical design of open-jet wind tunnel is based on the actual geometry of the wind tunnel. The commercially available ANSYS Fluent numerical code is used to study the

numerical model corresponding to the real geometry. Therefore, a good behavior of the numerical model will relatively agree with that of the actual tunnel. The governing equations are available in [11] and will not be presented here.

A. Solution method and boundary conditions

The commercial CFD code was applied to calculate the three-dimensional Reynolds-averaged Navier-Stokes (RANS) equations as well as the continuity equation. This code utilises the control-volume method alongside the Semi-Implicit Method for Pressure-Linked Equations (SIMPLEC) velocity-pressure coupling algorithm with the second order upwind discretisation. Furthermore, the numerical simulation was performed mainly on the basis of the standard k-epsilon model [5, 10, and 13]. **Table II** provides an overview of the CFD model boundary conditions. Furthermore, a large model of the whole wind tunnel was employed as shown in **Fig. 2**.

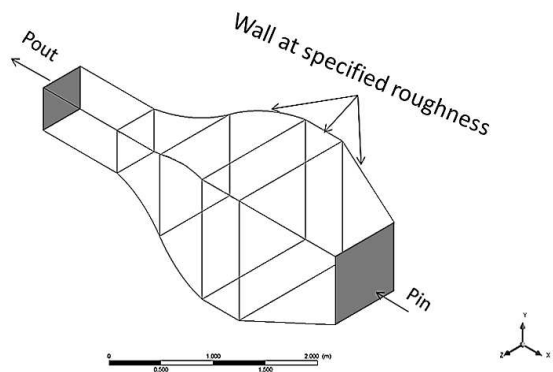


Fig. 2: Wind tunnel boundary condition in CFD.

Table II: The numerical simulation boundary conditions.

Parameters	Set value
Discretisation scheme	Second-order upwind
Algorithm	SIMPLEC
Time	Steady state
Intake fan (total pressure)	204 Pa
Pressure outlet	0 Pa
Gravity	-9.81

B. Mesh structure and mesh dependency

Structured prismatic mesh was applied to the wind tunnel sections with uncomplicated structure and one-dimensional flow. On the other hand, tetrahedral/hybrid cells were employed in sections such as the diffuser, and contraction, with complex structure and three-dimensional flow as shown in **Fig. 3**. The final number of mesh was 1518750 cells based on the mesh dependency study. Turbulent intensity and average velocity was set as monitored values against the number of cell. The convergence of the two parameters with 3-11% imbalances was achieved in the case of 506250 cells. Moreover, a rise in the value of interest resulted from the increase in the number of cells to 759375 cells. When the mesh size was increased even more, the simulation of the 1518750 cells produced a value situated in a satisfactory range, of 0.1-0.3%. What this implied was that the mesh resolution had no impact on the value of interest. Therefore,

to obtain results within the user-defined range, 1518750 cells were employed in additional analysis.

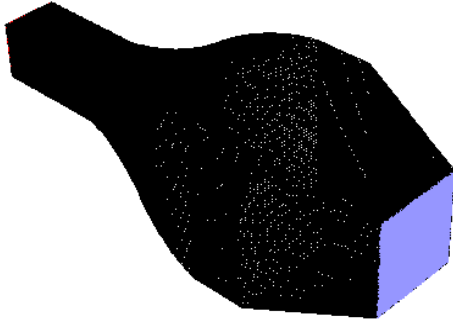


Fig. 3: Meshing imported to fluent software

V. EXPERIMENTAL APPARATUS

Two different sets of experiments are used in this paper depending on the experiments being performed. Initial investigations into an empty test section were carried out. This test was used to study the flow quality inside the test section e.g. turbulence intensity and flow symmetry compared to CFD results. The second set of experiments was used to investigate the un-actuated and actuated flow field over the convex hump model using an array of synthetic jet actuators. The experimental setup is shown in Fig. 4a and b.

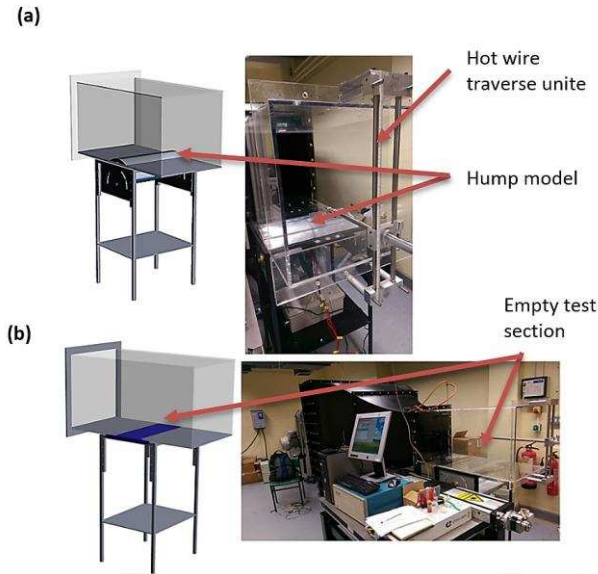


Fig. 4: a- Convex hump attached to the wind tunnel test section (solid works and real setup). b- Empty test section configurations (solid works and real setup).

The convex hump model selected (based on the CFD and flow visualization results) had a height of $h = 30$ mm, which represents the part facing the wind tunnel free stream air, span length (s) of 500 mm and hump radius curvature (R) of 181.7 mm. Fig. 5a clearly shows the main convex hump model and its removable parts. The figure clearly shows that the main hump model had two removable parts in order to facilitate the synthetic jet actuators and the function of rotating the hump (a "mushroom-like" shape), as shown in Fig. 5b. The first removable plate was used to accommodate 12 SJAs. This removable plate had a series of 12 embedded synthetic jet actuators, whilst maintaining the hump circular

profile. The curved face of the section contained 12 cavities, three orifices per cavity. This cavity had a maximum depth of 5.5mm with a maximum diameter of 32mm. A series of 1.2 mm diameter orifices was drilled out at the centre-line of the convex hump model. Each orifice had a 1.5 mm depth, since the extension of the whole cavity into the hump body with a depth of 24mm was 22.5mm. A close up view of a section of the removable part is presented in Fig. 5c, with four actuators and clamping being clearly seen. The synthetic jet actuators were fabricated at the University of Leeds. A FT-35T-2.6A1 piezo-ceramic diaphragm was used as a disk element. This formed the oscillatory surface essential to produce zero net mass-flow from each actuator (see Fig. 5c). The reason for using more than one orifice per cavity (three in this case) was to increase the strength and circulation of the vortex rings, which has been investigated in quiescent flow condition. The second removable part had a semi-triangular shape. This plate can be called as "stalk" removable plate that formed part of the rotating hump model. It is the main part of the rotating joint where the pivot bar (the trunnion) is inserted, which allowed the main hump to be rotated around its centre line up to ± 32 degrees. The pivot bar was positioned in a 25 mm diameter hole that represents the central rotation of the main hump model. The angles of rotation were monitored by a digital inclinometer protractor meter, upright magnet 360° slope angle which gives more accurate reading than normal graded protractors. The driving circuitry that supplies the signal to the piezo-ceramic diaphragms used consists of two components. The function generator is the first component, which allowed sine waveform, excitation frequency and amplitude to be altered as required. The output from the function generator was subjected to six power amplifiers (PDM-200). Each amplifier is able to provide a 20-times gain voltage amplitude. From this driving circuitry box, the signal then passed into the wires that travelled to each of the 12 actuators and oscillated the piezo-ceramic diaphragms.

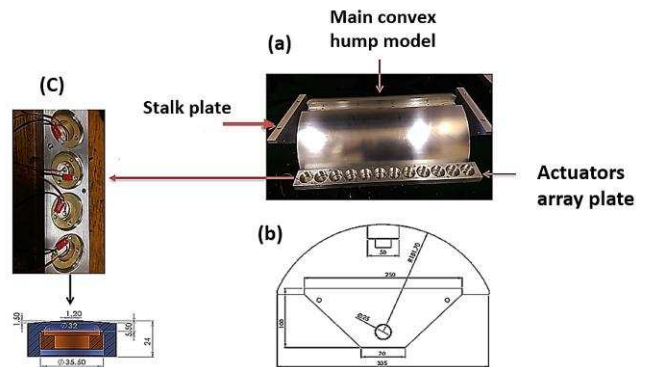


Fig. 5: a-The main convex hump model and its parts b-Convex hump dimensions, c- Close up view of four individual actuators showing (wire connections, a cross-section of single SJA dimensions, clamping piece).

VI. RESULTS AND DISCUSSIONS

A. Empty Test Section Results and Discussions

The purpose of the initial experiment should be conducted with an empty test section to measure the velocity inside the test section using a pitot static tube. The wind tunnel is designed to operate in an adjustable speed range from 3 m/s to greater than 20 m/s with motor frequency range from 5 Hz

up to 50 Hz. The variable frequency driver (VFD) responds to control signals from the remote keypad. The velocity has a linear fitted line against frequency as shown in **Fig. 6**, which clearly showed that the motor frequency increased linearly with the velocity of the wind tunnel. This test will help in any aerodynamic test in future such that any velocity can be selected with the corresponding motor frequency.

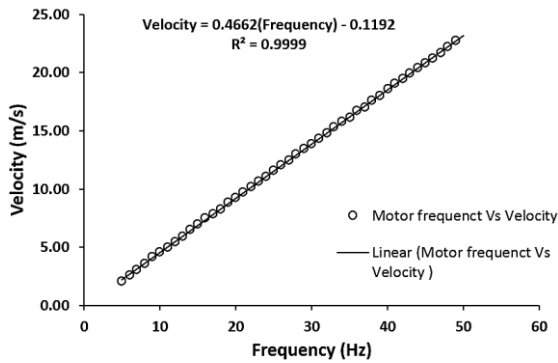


Fig. 6: Wind tunnel velocity vs frequency

In order to examine if the velocity distribution at the contraction exit and test section was homogeneous and had the desired turbulence intensity, the wind tunnel performance was tested using a single hot wire anemometer. Since wind tunnel flow quality can negatively affect experimental results, hence precise and steady flow quality measurements are significant, alongside with the understanding of the reasons and characteristic of flow turbulence in the wind tunnel. The experimental and CFD results of the turbulence intensity are explained in **Fig. 7a and b**. The figures clearly show the turbulence intensity of an empty wind tunnel at two planes and 6 lines in total as a function of the test section height. As expected, the turbulence intensity is significantly improved comparing to CFD results. The turbulence intensity shows the value of 1.8 % at a velocity of 19 m/s and then reduced to ~ 0.6 % when the boundary layer controllers were inserted. The most likely reason for this is due to the conditioning devices (honeycomb, mesh screen and settling chamber) that were carefully designed and inserted inside the wind tunnel, which not been considered in CFD model. This rise in turbulent intensity in CFD results is due to the flow separation on the wind tunnel corners that have a large impact on the flow quality inside the test section.

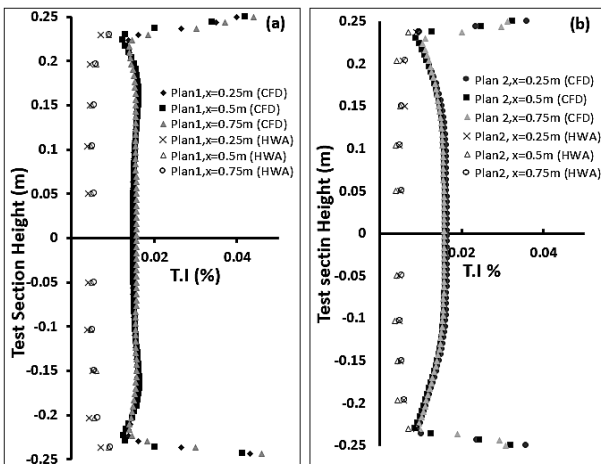


Fig. 7: The experimental and numerical turbulence intensity results in two planes (a- Plane 1, b- Plane 2, free stream velocity of 18 m/s).

The air velocity profile inside the all parts of an open jet wind tunnel is displayed in **Fig. 8**. No convex hump model and boundary layer controllers were considered. The velocity variation within the beginning and the end of the test section was higher (4.23%) as compared to the experimental case (1.78%) at a velocity of 19 m/s due to the flow separation on the wind tunnel corners. The combined boundary layer controllers (mesh screen and honeycomb) inside the wind tunnel significantly decreased the flow separation at the corners and enhanced the flow quality inside the test section. Therefore, as expected with a constructed wind tunnel, more uniform and symmetric flow was seen throughout the whole test section length and good general airflow distribution in the open jet wind tunnel circuit.

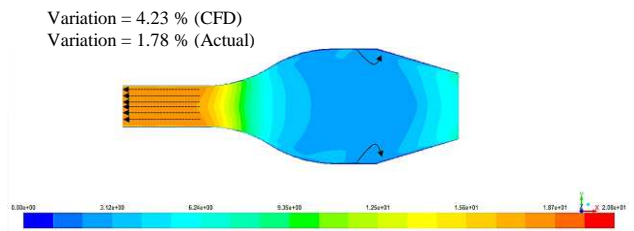


Fig. 8: Contour of velocity magnitude.

Moreover, a symmetric flow profile was seen in the wind tunnel test section as shown in **Fig. 9a and b** at locations of 0.25 m and 0.75m. Consequently, it can be established that the flow quality was approximately homogenous through the whole length of the test section.

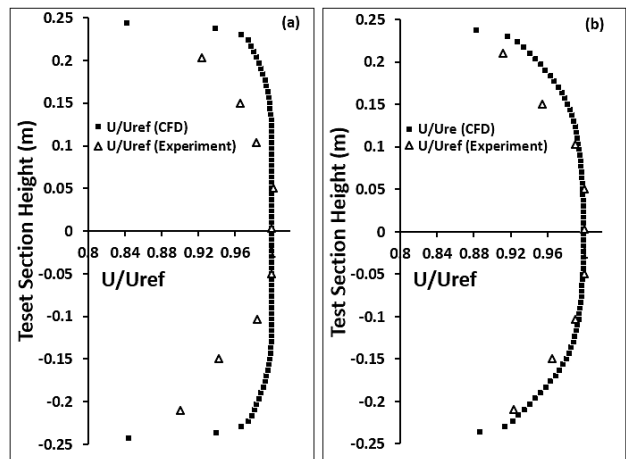


Fig. 9: Comparison between CFD and experimental data of the dimensionless velocity profile (a- at X = 0.75m and b- at X = 0.25m).

B. Actuated vs un-actuated wake flow behind the hump model

This section provides a study of power spectral density (PSD) and fluctuated velocity (U_{rms}) for the un-actuated hump. Then, the alteration to the wake flow behind the convex hump induced by an array of SJAs is investigated. To reduce the number of results, three parameters were kept constant during the experiments. The free stream velocity was fixed to $U_{\infty} = 7$ m/s, $X/L = 0.05$, Y/h ranged from 0.033 to 3.2. A not to scale of these parameters and measurement region are explained in **Fig. 10** in more detail. In keeping with the Helmholtz frequency of the cavity, a driving frequency of 1000 Hz was established to avoid the damage

to the piezoceramic diaphragm. Three jet-to-free stream velocity ratios (0.5, 1, and 1.5) were compared such that each jet velocity was measured in quiescent conditions, before being subjected to external cross flow.

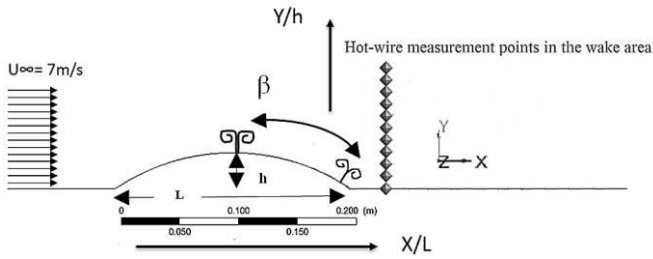


Fig. 10: Actuated vs un-actuated measurements setup behind the convex hump.

In order to facilitate comparisons between the actuated and un-actuated cases, the PSD and Urms results for the un-actuated hump case are shown in **Fig. 11a and b**. As shown in **Fig. 11a**, a dominant spectral peak at a Strouhal number $St_h = 0.3$ acquired from the PSD with the un-actuated hump. This peak is generally broadband in nature which is accompanied by Karman vortex shedding from the separated flow region. While, **Fig. 11b** clearly showed the single peak distribution of the fluctuated velocity associated with the shear layer on one side of the wake. The highest fluctuation in velocity occurred around $Y/h = 0.5$ for the un-actuated case.

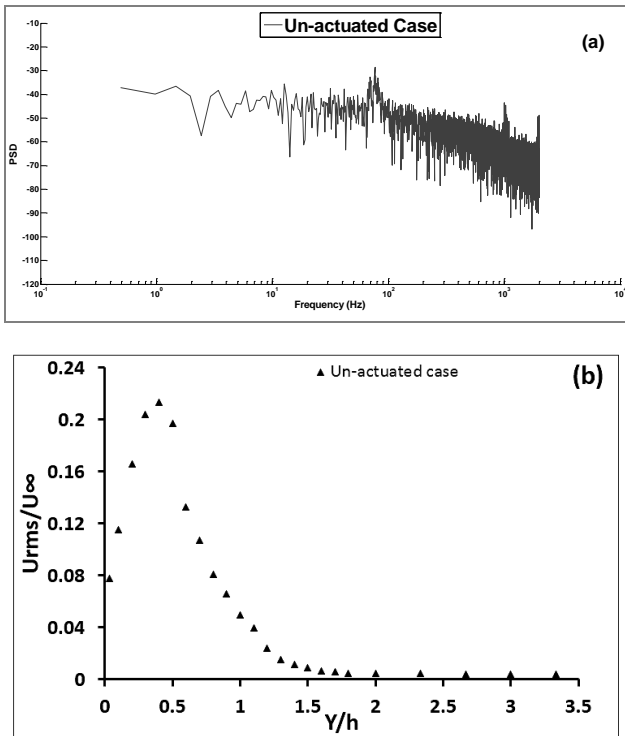


Fig. 11: a- PSD, b- Fluctuated velocity (Urms) for the un-actuated case.

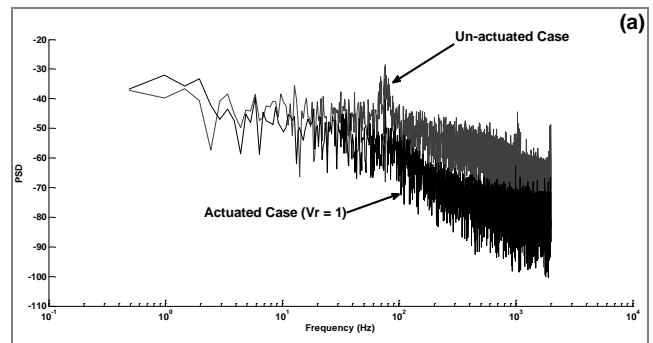
When the synthetic jet is activated, it affects both PSD and fluctuated velocity. **Fig. 12 a, and b** compare the characteristics of PSD under un-actuated and actuated hump flow field. From the results, it can be noticed that the effect of synthetic jets on PSD was only seen at an angular position of jet actuation of $\beta = 10^\circ$ suggesting that the actuation was just upstream of the separation point and had the big impact

of PSD. However, the effect of synthetic jets on the velocity fluctuation (U_{rms}) in the wake flow was seen to be reduced as both β and V_r increased.

As can be deduced from the results, comparing to the un-actuated case, the synthetic jet actuation had no impact that can be seen on the dominant peak frequency at $V_r = 0.5$ (not presented here), meaning that the prevailing effect of the free-stream flow caused rapid deflection and loss structure of the jet. On the other hand, at $V_r = 1$ and 1.5, the interaction between the synthetic jets and the free shear layers led to a decrease in the vortex shedding frequency. The control cases were compared at $V_r = 0.5$ with $V_r = 1, 1.5$, findings showing that the free-stream flow could be shifted by the jet at $V_r = 1$ and 1.5 because it had greater strength. Furthermore, by comparison to the un-actuated case, the figures clearly show that the turbulent energy was reduced by the developing of vortex ring, resulting in the shear layer frequency to decrease too.

Further analyses were conducted to shed more light on the SJA impact on the hump wake region. Thus, the following sections address the actuation impact on the fluctuated velocity in the wake region. **Fig. 12c** clearly shows that when the synthetic jets are activated, the velocity deficit in the wake area was altered by the addition of single sine wave. The effect of varying the velocity ratio can be clearly seen. For instance, an increase in the velocity ratio (V_r) considerably reduced the fluctuated velocity in the wake area with an optimum angular position of actuation angle of $\beta = 30^\circ$. At a velocity ratio of 0.5, actuation had a smaller yet clear effect on the fluctuated velocity in the wake area, phenomenon which occurred in every angle.

At a velocity ratio of 1, there was a decrease in the fluctuated velocity ratio U_{mean}/U_∞ in the wake area from 0.205 to 0.191, whilst at a velocity ratio of 1.5, there was around 10% reduction in the fluctuating velocity in the wake area compared to the un-actuated case. It is apparent from the results that the rise in the velocity ratio determined a substantial decrease in the wake velocity fluctuation (U_{rms}) as a result of synthetic jet actuation control, which could induce a decrease in drag force that needs further investigations.



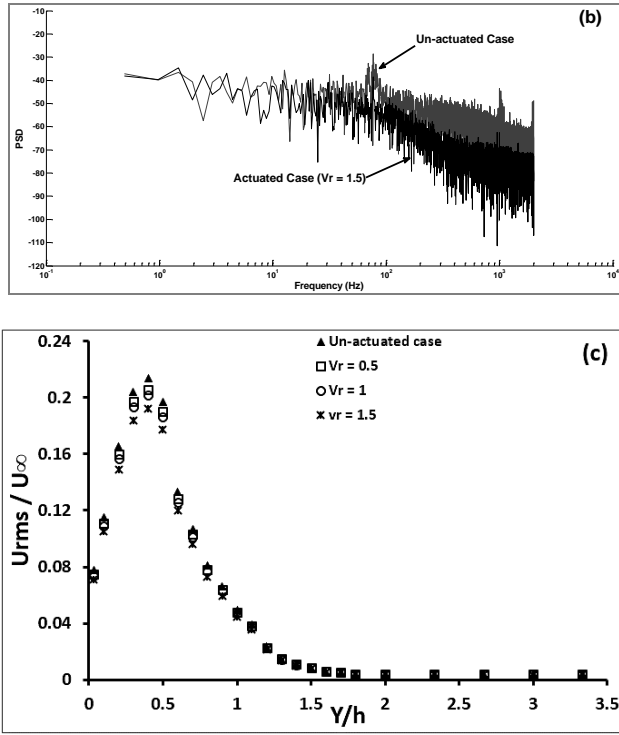


Fig. 12: Actuated vs un-actuated cases, a- PSD at $V_r = 1$, $\beta = 10^\circ$; b- PSD at $V_r = 1.5$, $\beta = 10^\circ$ and c- Urms at $\beta = 30^\circ$ V_r 0.5, 1, and 1.5.

VII. CONCLUSION AND FUTURE WORK

A new low-speed open-jet wind tunnel has been designed and constructed at the University of Leeds. Analysis of the flow quality results in an empty test section showed that adding flow conditioning devices (mesh screen and honeycomb) to the wind tunnel reduced the turbulent intensity from 1.8% to 0.6% at 19m/s. This clearly indicates that the quality of flow in the test section was greatly affected by flow conditioning devices. Hence, special care should be given while designing the boundary layer controller at settling chamber mainly the section in-line with the test section.

Moreover, the velocity fluctuation (Urms) profile and PSD behind the convex hump were measured, with and without actuation using an array of SJAs as active flow control. The fluctuated velocity profile (Urms) is modified by the synthetic jet actuation to be reduced in the wake region. This might indicate that the velocity deficit in the wake area is decreased and flow separation is delayed. Both actuated and un-actuated power spectral density was presented at $V_r = 1$, 1.5 and $\beta = 10^\circ$. The comparison of the PSD control cases at $V_r = 1$ and $V_r = 1.5$ suggest that the synthetic can reduce the dominated peak frequency. However, the effect of synthetic jets on the velocity fluctuation (Urms) in the wake flow was seen to be reduced at $\beta_{opt} = 30^\circ$ as V_r increased from 0.5 to 1.5.

However, an additional investigation of representing the mesh screens and honeycomb as a porous domain in CFD would further improve the predicting of T.I in the test section. Moreover, the effect of the synthetic jets on the hump flow field at different tunnel velocity and different excitation waveform using both HWA and PIV are ongoing to achieve more information about the wake area. Additional investigation of pressure distribution measurements is needed to identify drag reduction or lift enhancement.

APPENDIX

Table III: Flow measurements and its relation formulas

Measurements	Related Formula	Definition
Velocity Ratio (V_r)	U_j/U_∞	U_j : Jet velocity U_∞ : Stream velocity
Turbulent Intensity	B/U_∞	B : Standard deviation
Dimensionless Velocity	U/U_{ref}	U : Velocity magnitude U_{ref} : Maximum velocity
Strouhal Number (St h)	fh/U_∞	f : Shear layer frequency shedding h : Hump height

ACKNOWLEDGMENT

The construction of open jet wind tunnel is funded by University of Leeds (School of Civil Engineering). Authors gratefully acknowledge the financial support by the institution. The first author wants to express his gratitude to Iraqi organizations (HCED and University of Diyala) for their financial support during the PhD study.

REFERENCES

- [1] Barlow, J. B., W. H. Rae, and A. Pope. "Low-speed wind tunnel testing, 1999." Jhon Wiley & Sons, Canada.
- [2] Mehta, R., Bradshaw P., "Design rules for small low-speed wind tunnels." Aeronautical Journal 83.827 (1979): 443-449.
- [3] Ghani, S., Aroussi A., Rice E., "Simulation of road vehicle natural environment in a climatic wind tunnel." simulation practice and theory 8.6 (2001): 359-375.
- [4] Launder, B., Brian D., "Lectures in mathematical models of turbulence." (1972), Academic Press, London, UK.
- [5] Gartmann, A., Wolfgang F., Wolfgang S., and Mathias D., "CFD modelling and validation of measured wind field data in a portable wind tunnel." Aeolian Research 3, no. 3 (2011): 315-325.
- [6] Sathapornanon, S., Aryut W., Somchai T., Monchai L., Alongkorn Pimpin, and Asi B., "The Design and Development of The FMRL 60x18 cm² Wide-Angle Screened-Diffuser Blower Tunnel, Part II: The Screened Diffuser." In Proceedings of The Thirteenth National Mechanical Engineering Conference, Pattaya, Chonburi, Thailand, vol. 2, pp. 27-37. 1999.
- [7] Clauser, F., "Turbulent boundary layers in adverse pressure gradients." Journal of the Aeronautical Sciences (2012).
- [8] Westphal, R., Eaton J., Pauley W., "Interaction between a vortex and a turbulent boundary layer in a streamwise pressure gradient." Turbulent Shear Flows 5. Springer Berlin Heidelberg, 1987. 266-277.
- [9] Schwarz, W., and Peter B., "Measurements in a pressure-driven three-dimensional turbulent boundary layer during development and decay." AIAA journal 31, no. 7 (1993): 1207-1214.
- [10] Calautit, J. K., Hassam N., Ch., Ben R. H., Lik F. S., "A validated design methodology for a closed-loop subsonic wind tunnel." Journal of Wind Engineering and Industrial Aerodynamics 125 (2014): 180-194.
- [11] FLUENT Incorporated: FLUENT user guide [online] 2006. Available from: www1.ansys.com (accessed 01.02.12).
- [12] Vljajnac, M., "Design, construction and evaluation of a subsonic wind tunnel." PhD diss., Massachusetts Institute of Technology, 1970.
- [13] Moonen, P., Bert B., Staf R., and Jan C., "Numerical modeling of the flow conditions in a closed-circuit low-speed wind tunnel", Journal of Wind Engineering and Industrial Aerodynamics 94, no. 10 (2006): 699-723.